journal

J. Am. Ceram. Soc., 85 [4] 780–86 (2002)

Determination of Binder Decomposition Kinetics for Specifying Heating Parameters in Binder Burnout Cycles

Rajesh V. Shende and Stephen J. Lombardo*

Department of Chemical Engineering, University of Missouri, Columbia, Missouri 65211

The decomposition kinetics of poly(vinyl butyral) binder from barium titanate multilayer ceramic capacitors with platinum metal electrodes were analyzed by thermogravimetric analysis as a function of the heating rate. The activation energy and pre-exponential factor for the decomposition kinetics were determined from two types of integral equations, from the Redhead method, and from the variation in heating rate method. The accuracy of the kinetic parameters determined from these methods was then evaluated for describing the observed rate of binder decomposition. Although the individual models yielded very different kinetic parameters, all were capable of describing the experimental data within ±15% accuracy. The kinetic parameters were then used in a coupled transport and kinetic model for describing the buildup of pressure within the ceramic green body as a function of the heating cycle. A methodology based on calculus of variations was also developed to predict the minimum duration for the binder burnout cycle.

I. Introduction

DURING the processing of ceramic green bodies, thermal decomposition[1] of polymers is often used to convert solid-phase binder into gas-phase decomposition products. When the pressure associated with the decomposition products becomes too high, defects may be introduced into the green body or fracture of the component may occur. To avoid the formation of such defects, slow heating cycles with multiple hold periods are used, and as a consequence, binder removal cycles are often the single longest processing operation for which the total duration may be hundreds of hours. The selection of heating rates, hold temperatures, and hold times for binder burnout cycles thus becomes important so as to maximize yield in a minimum of furnace time.

One approach to provide insight into binder burnout is to measure the decomposition kinetics of the binder[2,3] with a thermogravimetric analyzer (TGA) and then to use the weight loss data to establish the heating cycle. Although the study of weight loss on small quantities of material in a TGA can yield the decomposition kinetics prevailing when no mass-transport limitations exist, the use of these results to specify furnace cycles for real components is not straightforward. One possible strategy is to use the intrinsic burnout kinetics with coupled kinetic and transport models[4–17] to describe the evolution of pressure within the body, and then to use the pressure increase as a guide to specifying the burnout cycle. With this approach, accurate determination of the activation energy and preexponential factor is a necessary first step to predict the evolution of pressure within the body.

Although the degradation pathways of pure polymers can be classified as unzipping, random scission, and oxidative degradation, the actual mechanisms of binder degradation from real components are more complicated[1] and depend on catalytic effects between ceramic particles and binder, on the atmosphere, and for multilayer ceramic capacitors (MLCs), on the metal electrode material.[15] These mechanisms are complex, as has been observed for poly(vinyl butyral),[1,15] poly(ethylene oxide),[18] and ethylene vinyl acetate.[19]

In this study, we examine the decomposition kinetics of a poly(vinyl butyral) (PVB) binder from barium titanate MLCs containing platinum as the electrode material. We show how the heating rate used in the TGA experiments has a strong influence on the observed decomposition behavior and how different kinetic models can be used to determine the activation energy and pre-exponential factor for the rate of binder degradation. These kinetic parameters are then incorporated into a transport model for predicting the increase in pressure within a ceramic green body. We further show the effect that the selection of heating rates, hold temperatures, and hold times has on the buildup of pressure within the component as a function of the length scale of the body. Finally, we develop a methodology for determining the minimum duration of the binder burnout cycle.

II. Experimental Procedure

Green tapes composed of barium titanate powder (Tamtron X7R412H, TAM Ceramics, Inc., Niagara Falls, NY) and a PVB binder solution (B73305 Ferro Corp., San Marcos, CA) were used in this study. The individual tapes, nominally 300 μm thick, were laminated into MLCs at 2–4 MPa and 80°–85°C with platinum paste (E1192 Ferro Corp., San Marcos, CA) screen-printed at a thickness of nominally 5–10 μm. The binder fraction was ~10% of the total sample weight.

The weight loss experiments were conducted with a TGA (Model 1020 Series TGA 7, Perkin-Elmer Corp., Norwalk, CT) interfaced with Fourier transform infrared spectrometery (FTIR; Model 2000, Perkin-Elmer), the details of which have been described elsewhere.[20] Typically, 50 mg of sample were loaded into the TGA, and the flow rate of the carrier gas, air, was set at 90 cm^3/min.

III. Results and Discussion

(1) Kinetic Analysis of TGA Data

The evolution of binder weight loss as a function of temperature is displayed in Fig. 1 for four heating rates. At a heating rate of 1°C/min, the weight loss becomes rapid at 150°C, and a break in the curve is observed at 210°C. As the heating rate is increased, the weight loss profiles are shifted to higher temperatures and the region of rapid binder degradation is seen to be a function of the heating rate. For a heating rate of 1°C/min, 50% conversion occurs at ~180°C, whereas for a heating rate of 20°C/min, 50% conversion occurs at an ~100°C higher temperature. The decomposition data in Fig. 1 thus indicate that the steep region of binder weight loss depends strongly on the heating rate used in the TGA experiment, and thus these data are not directly useful for specifying heating rates and hold temperatures for binder removal cycles.

An alternative representation of TGA weight loss profiles is to take the first derivative of the experimental traces. With this

L. Bergstrom—contributing editor

Manuscript No. 187907. Received February 26, 2001; approved November 26, 2001.

*Member, American Ceramic Society.

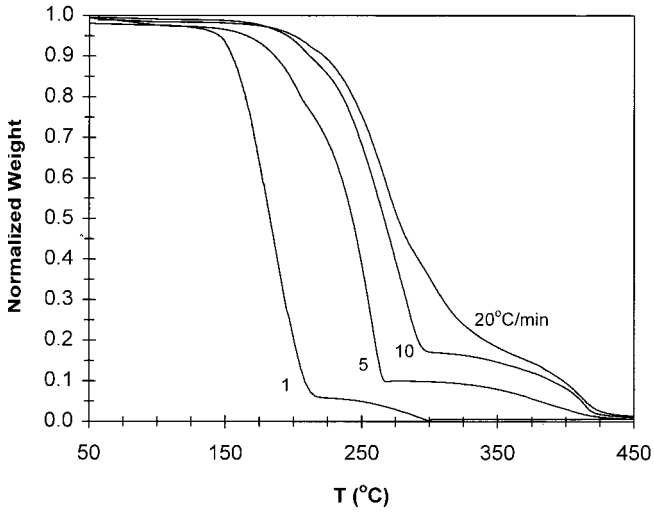

Fig. 1. Weight loss profiles of a 10 wt% PVB–$BaTiO_3$–Pt composition during TGA experiments for different heating rates in air.

representation of the data (see Fig. 2), the major regions of binder decomposition appear as peaks and the positions of the peaks correspond to the points of inflection in the curves in Fig. 1. For the experiments conducted on the PVB–$BaTiO_3$–Pt MLCs, two peaks are observed for each heating rate; as the heating rate is increased, the peak positions are shifted to higher temperatures.

The composition of the binder degradation products was assessed by FTIR analysis of the gas phase effluent from the TGA furnace for experiments conducted at 10°C/min. Figure 3, a stacked plot of infrared absorbance versus wavenumber at successive temperatures, shows that a number of species are evolved at different temperatures. The major regions of absorbance are at 2350 cm^{-1} (CO_2), at 1680–1750 cm^{-1} (carbonyl stretches), at 2700–3000 (C-H stretches), and at 3550–3650 (hydroxyl stretches). These spectra have been deconvoluted elsewhere,[15] and the mechanism of binder decomposition that arises is the following. At low temperature of ~100°C, CO_2 is first evolved, followed by C_4 species containing carbonyl vibrations (butanal, butenal, butanoic acid, and butanol). The evolution of CO_2 and C_4 species occurs at conversions to 85%, which is approximately at the break in the corresponding TGA curve in Fig. 1. At still higher temperature, only a CO_2 peak is observed, which corresponds to the last 15% of binder decomposition.

Both the weight loss and FTIR data indicate that the kinetics of binder decomposition are complex when both ceramic and a noble

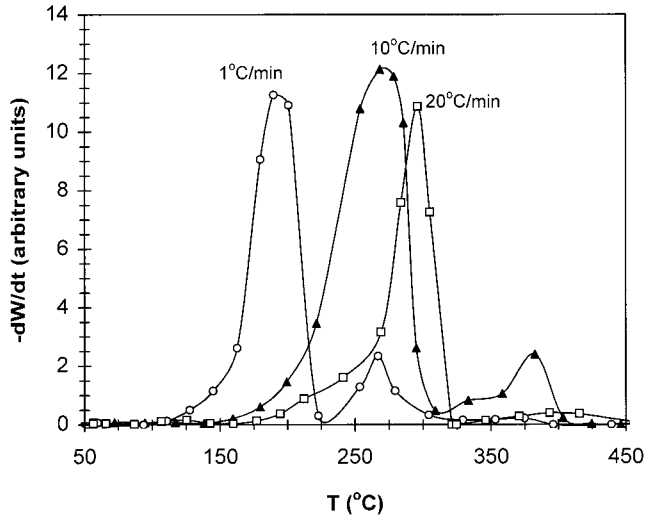

Fig. 2. First derivative TGA profiles of a PVB–$BaTiO_3$–Pt composition for different heating rates in air.

metal such as platinum are present. Although the TGA and FTIR data in combination provide some insight into binder degradation, the exact details of the decomposition mechanism, such as bond breakage and short-lived chemical intermediates, remain unresolved. The precise nature of the mechanism is not, however, of primary interest for establishing binder burnout cycles. Rather, the binder is a fugitive species whose removal in a timely manner with no damage to the sample is of importance. An accurate representation of the rate of weight loss is, however, needed to predict the buildup of pressure within the green ceramic body.

The analysis of TGA weight loss data to extract kinetic parameters has been the subject of several studies and has been examined in detail elsewhere.[21–24] In this work, we will analyze the TGA data by a number of methods to assess their accuracy in representing the experimental results. One analysis approach to determine the activation energy, E, and pre-exponential factor, A, from TGA data is to assume or establish a model for the decomposition mechanism as a function of conversion and then to use the model with an integral form of the kinetic expression. For a general kinetic process, $f(\alpha)$, where α is the fraction of reacted binder, the rate expression for a thermally activated process can be represented as

$$\frac{d\alpha}{dt} = A \exp\left[\frac{-E}{RT}\right] f(\alpha) \tag{1}$$

where T is the temperature and R is the gas constant. When TGA experiments are conducted with a constant heating rate, β, the activation energy and pre-exponential factor can be determined from the integral method of Lee and Beck[22]:

$$\ln\left[\frac{F(\alpha)}{T^2}\right] = \ln\left[\frac{AR}{\beta(E + 2RT)}\right] - \frac{E}{RT} \tag{2}$$

where $F(\alpha)$ is the integrated form of $f(\alpha)$. Although many forms of $f(\alpha)$ and hence $F(\alpha)$ have been proposed, we will evaluate two: for first-order decomposition kinetics, $f(\alpha) = (1 - \alpha)$ and $F(\alpha) = -\ln(1 - \alpha)$; for a diffusion-controlled process, $f(\alpha) = 3(1 - \alpha)^{1/3}/[2(1 - \alpha)^{-1/3} - 1]$ and $F(\alpha) = (1 - (1 - \alpha)^{1/3})^2$. From inspection of the forms of $F(\alpha)$, we can expect that the kinetic parameters determined by these two methods will be different.

Two other methods for determining the kinetic parameters are to use weight loss data in the form shown in Fig. 2 to determine the peak temperatures, T_p. For the Redhead method,[21] only a single first derivative trace is needed, and for an assumed value of the pre-exponential factor, the activation energy is determined from

$$\frac{E}{RT_p^2} = \frac{A}{\beta} \exp\left(-\frac{E}{RT_p}\right) \tag{3}$$

For the variation in the heating rate method,[24] first-derivative TGA data are obtained at multiple heating rates, as shown in Fig. 2. The peak positions as a function of the heating rate are then used with

$$2 \ln T_p - \ln \beta = \frac{E}{RT_p} + \ln\left(\frac{E}{AR}\right) \tag{4}$$

to obtain values of A and E.

The kinetic parameters determined by these techniques for the major region of binder decomposition are summarized in Table I. Depending on the model used, the activation energies and pre-exponential factors vary by a considerable amount. In general, though, a compensation effect[25] is evident whereby large values of the pre-exponential factor arise with large values of the activation energy. For those methods that lead to linear behavior in the analysis, the linear regression coefficients, r^2, are also shown in Table I, and they are typically >0.98.

The kinetic parameters in Table I have been used to simulate binder weight loss for a heating rate of 10°C/min. Figure 4 illustrates that the parameters determined from both of the integral methods predict quite closely the degree of binder weight loss observed in the TGA experiments. The kinetic parameters determined by the variation

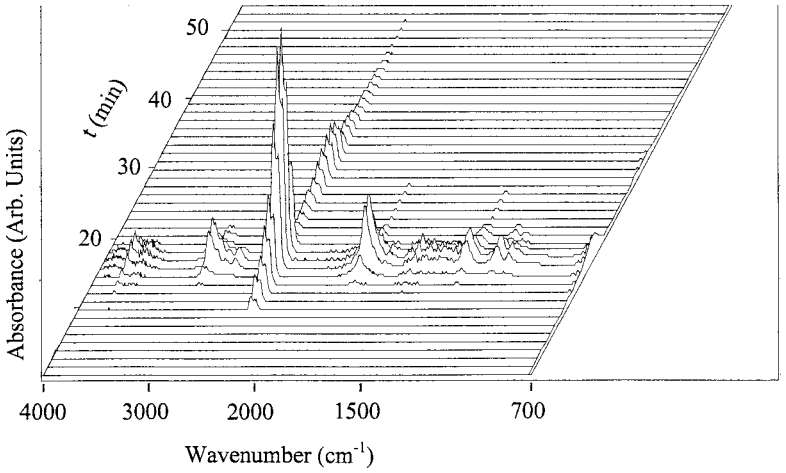

Fig. 3. Stacked plot of FTIR absorbance spectra recorded during a TGA experiment in air at a heating rate of 10°C/min. Sample was a PVB–$BaTiO_3$–Pt composition.

in heating rate method and the method of Redhead are less satisfactory than the integral methods. This degree of accuracy extends to all the heating rates evaluated here. That the integral methods do a superior job of representing the weight loss data are to be expected because all the TGA data are used in the analysis, whereas for methods based on peak position, only a single point per peak is used. What is interesting is that despite the very different mechanisms underlying the first-order and diffusion-controlled models, and hence very different kinetic parameters, each integral method leads to kinetic parameters that can be used to give a reasonable representation of the rate of binder decomposition.

The lack of one markedly better set of kinetic constants is not surprising. Despite the TGA/FTIR analysis of binder decomposition, the complete kinetic pathway in terms of bond breakage and reaction intermediates is still not fully understood. In addition, the architectures of the MLC is not homogeneous when viewed at different length scales. Different regions of the MLC contain different amounts of ceramic and binder; metal and binder; and ceramic, metal, and binder. These regions all have very different rates of decomposition.[15] In light of the complexity of the mechanism and the inhomogeneous nature of the substrate, the activation energies and pre-exponential factors appearing in Table I must be regarded as lumped or apparent kinetic constants, because it is not possible to analyze separately the pathways corresponding to the appearance of each individual decomposition product from each region of the sample. Despite this limitation, the kinetic parameters are reasonable representations of the macroscopic rate of binder decomposition, and this is what is important in modeling the buildup of pressure within porous bodies.

Further inspection of the values of A and E appearing in Table I indicates that they vary substantially with the heating rate, and thus a unique set of A and E does not arise from such analyses. Figure 5 illustrates that when the kinetic parameters determined from TGA experiments conducted at 10°C/min are used to simulate experiments conducted at 5°C/min, the level of agreement between model calculations and experimental results is poorer. The two best sets of kinetic constants for this case arise from the first-order integral method and the variation in the heating-rate method. When similar simulations are conducted with other sets of experimental data and kinetic parameters obtained at different values of the heating rate, the same reduction in

Table I. Activation Energies and Pre-Exponential Factors as a Function of Linear Heating Rate and Method of Analysis

β (°C/min)	A (s^{-1})	E (kJ/mol)	r^2	$1-\alpha$
	Integral method (first-order)			
0.2	8.5×10^{15}	151.0	0.99	0.96–0.63
1	2.34×10^{7}	92.5	0.99	0.96–0.09
5	7.37×10^{3}	64.3	0.98	0.94–0.10
10	8.19×10^{3}	65.8	0.99	0.99–0.21
20	4.50×10^{3}	61.9	0.99	0.97–0.47
	Integral method (diffusion)			
1	8.11×10^{15}	176.0	0.99	0.96–0.09
5	1.05×10^{9}	124.5	0.99	0.94–0.09
10	3.36×10^{9}	133.7	1.00	0.98–0.21
20	9.23×10^{8}	127.8	0.99	0.97–0.47
	Variation in heating rate (first-order)			
1	2.62×10^{3}	60.5	0.99	1.0–0
5	3.38×10^{3}	60.5	0.99	1.0–0
10	2.75×10^{3}	60.5	0.99	1.0–0
20	2.71×10^{3}	60.5	0.99	1.0–0
	Redhead (first-order)			
1	1.00×10^{8}	100.0		1.0–0
5	1.00×10^{8}	102.2		1.0–0
10	1.00×10^{8}	105.4		1.0–0
20	1.00×10^{8}	107.6		1.0–0

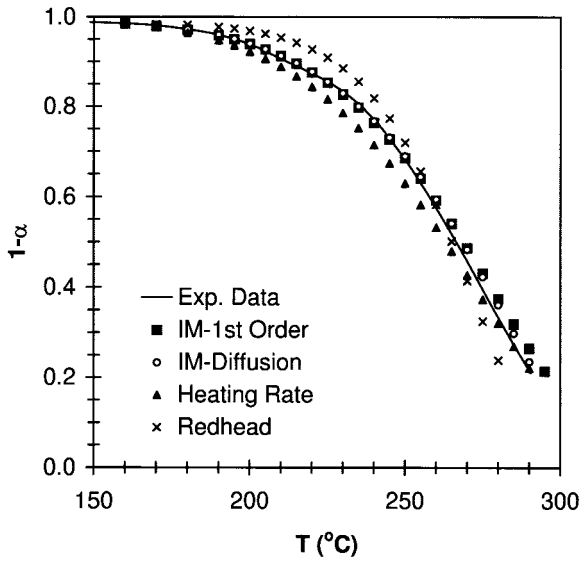

Fig. 4. Comparison of an experimental TGA weight loss profile (solid line) recorded at 10°C/min with the kinetics simulated by the four models using the parameters obtained by analyzing TGA data taken at 10°C/min. The sample was a PVB–$BaTiO_3$–Pt composition. IM denotes integral method.

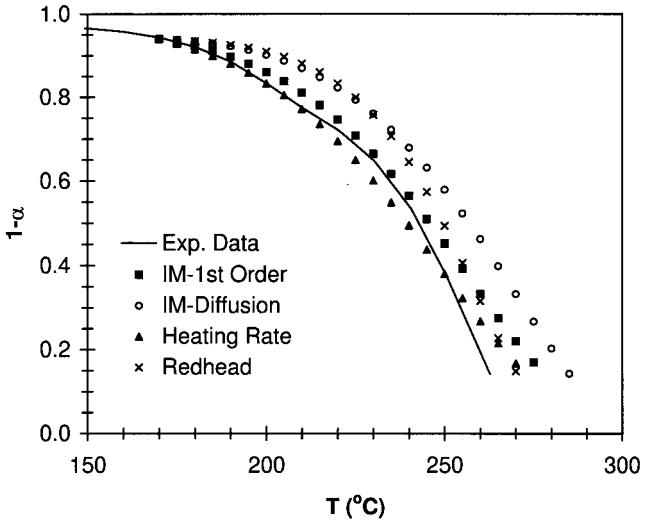

Fig. 5. Comparison of an experimental TGA weight loss profile (solid line) recorded at 5°C/min with the kinetics simulated by the four models using the parameters obtained by analyzing TGA data taken at 10°C/min. The sample was a PVB–$BaTiO_3$–Pt composition. IM denotes integral method.

accuracy is observed. In general, we find that the kinetic parameters determined from the variation in heating rate method are better for predicting the experimental data over a range of temperature, presumably because data from all the heating rates are used in the analysis.

The trends in Fig. 5 thus suggest that in the absence of certainty in the decomposition mechanism, use of kinetic parameters extracted from TGA data taken at one heating rate for prediction of the decomposition kinetics taken at another heating rate must be done with caution. It was for this reason that the simulations in Ref. 15 were conducted with kinetic parameters (see Table I) taken from TGA data conducted at heating rates of 0.2°C/min, which is more representative of the slow heating rates typically used in binder burnout cycles. In general, to obtain an accurate description of the kinetics of binder decomposition, measurements of weight loss should be made on samples representative of the composition that will be used for the actual components and over the temperature range where binder burnout will be conducted. The weight loss data can then be analyzed by the methods described earlier to obtain the kinetic parameters.

(2) Modeling of Pressure Buildup

To predict the buildup of pressure within porous compacts, we have developed a coupled transport and kinetic model as a function of time, t, and spatial coordinate, x, as[15]

$$\frac{\partial(V_g\rho)}{\partial t} = -\frac{\partial}{\partial x}(\rho u) + \frac{r(x,t)}{M} \tag{5}$$

where V_g is the fraction of the body occupied by gas, ρ is the molar gas density, $r(x,t)$ is the reaction rate, and M is the average molecular weight of the gas-phase products. The superficial velocity, u, appearing in Eq. (5) can be represented by Darcy's law

$$u = -\frac{\kappa}{\mu}\frac{\partial P}{\partial x} \tag{6}$$

where μ is the viscosity of the gas. The permeability of the gas in the pore space, κ, appearing in Eq. (6) is most simply represented by the Kozeny–Carman form

$$\kappa = \frac{V_g^3}{k(1-V_g)^2 S^2} \tag{7}$$

where k is a constant accounting for the shape and tortuosity of the pores, and S is the surface area per unit volume of the body. For the particle size of ~0.1–1 μm, the range of pore sizes of 0.01–0.1 μm corresponds to the slip flow regime, and thus the velocity in Eq. (6) can be corrected to account for this.[26,27]

As binder decomposes within the body, the volume fraction of binder, V_b, decreases with time. For a constant density of polymer, ρ_b, the change in volume fraction of binder is proportional to the reaction rate and can be determined from conservation of mass:

$$V_b(x,t) = V_{b,o} - \int_0^t \frac{r(x,t)}{\rho_b}\,dt \tag{8}$$

where $V_{b,o}$ is the initial volume fraction of binder. Because the volume fraction of binder, V_b, can be determined from Eq. (8), the volume fraction of the body occupied by gas, V_g, is given by

$$V_g = 1 - V_s - V_b \tag{9}$$

where V_s is the volume fraction of ceramic in the green body.

For the slow heating rates typically used in binder burnout cycles, gradients in temperature and binder concentration are often small.[13,15] These observations, along with use of the pseudosteady-state assumption, then lead to an analytical solution to Eq. (5). This solution describes the buildup of relative pressure within the center of a body, $(P/P_o)_o$, as a function of the body half-length, L, as[15]

$$\left(\frac{P}{P_o}\right)_o = \left[1 + \frac{\mu k S^2 RT}{MP_o^2}\frac{(1-V_g)^2}{V_g^3}\,r(x,t)\,L^2\right]^{1/2} \tag{10}$$

provided that the kinetics $r(x,t)$ have been determined.

Equations (5)–(10) were solved by a finite-difference method for a linear heating rate $\beta = dT/dt$ to determine the pressure in the center of the ceramic body as a function of temperature. The values of the quantities appearing in Eqs. (5)–(10) are $T_o = 300$ K, $P_o = 0.1$ MPa, $V_{b,o} = 0.3$, $V_s = 0.5$, $\rho_b = 1000$ kg/m^3, $M = 44$ g/mol, $\mu = 0.025 \times 10^{-3}$ Pa·s, $S = 6 \times 10^6$ m^{-1}, and $k = 5$. The kinetic parameters to describe the binder decomposition used are those listed in Table I, which were determined from the first-order integral method at a heating rate of 0.2°C/min.

The evolution of $(P/P_o)_o$ as a function of heating rate is shown in Fig. 6 for a body of $L = 1$ cm. For a heating rate of 0.01°C/min, the maximum in $(P/P_o)_o$ is very close to unity and occurs at 92°C. As the heating rate is increased, the magnitude of $(P/P_o)_o$ also increases, and the maximum occurs at progressively higher temperatures. Also contained in Fig. 6 is the simulated profiles of binder-volume fraction as a function of temperature, which are

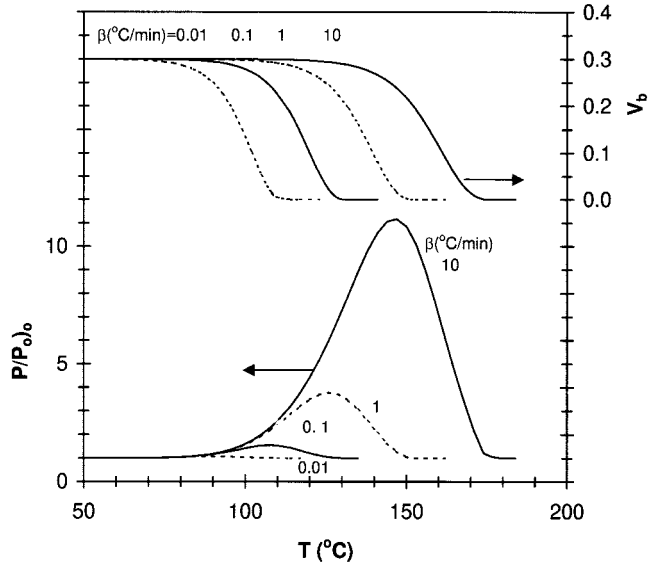

Fig. 6. Simulated pressure ratio at the center of the body and volume fraction of binder as a function of heating rate for a body of $L = 1$ cm.

analogous to the TGA traces of binder weight loss in Fig. 1. Careful comparison of the trends in Fig. 6 indicates that the maximum in $(P/P_o)_o$ always occurs at lower temperatures than do the temperatures at which the points of inflection in the TGA curves occur. In fact, the maximum in $(P/P_o)_o$ occurs when the conversion of binder is relatively low, at 20%. When the body of the sample is increased to $L = 2$ cm length, the maximum in $(P/P_o)_o$ at a heating rate of 10°C/min occurs at approximately the same temperature as for a body of 1 cm length, but the magnitude is now twice as large.

Figure 7 shows how the pressure at the center of the body, $(P/P_o)_o$, varies with volume fraction of binder as a function of hold temperature and body dimension. The pressure in the center of the body is seen to decrease as the volume fraction of binder decreases with time. The strong dependence of pressure buildup on both the hold temperature and body dimension is evident. Figure 7 can be used in the following fashion to specify hold temperatures when the threshold pressure ratio is known, below which the sample must remain. For example, if the threshold value of $(P/P_o)_o = 4$, then the first hold for a body of $L = 4$ cm in length can be placed at 95°C. Placing the hold at only 10°C higher at 105°C would lead to more than two times the threshold value. If, however, the body length is $L = 1$ cm, then the first hold can be placed at 105°C while still remaining below the threshold pressure ratio of four. Figure 7 thus highlights the sensitivity of pressure buildup in the burnout cycle to both the hold temperature and body size.

The procedure outlined above is useful for specifying the temperature of the first hold period. To specify the duration, it is necessary to refer to a plot such as Fig. 8, where we show the evolution of $(P/P_o)_o$ with hold time as a function of hold temperature and body dimension. The maximum pressure is seen to decrease with time, and these trends can be used in the following manner: if a body of $L = 4$ cm has a threshold pressure of $(P/P_o)_o = 4$, then the first hold can be placed at 95°C. After 7 h at this temperature, the pressure and volume fraction of binder will have decreased sufficiently so that the temperature can then be ramped to 105°C, thereby increasing the rate of binder decomposition while still remaining below the threshold value of $(P/P_o)_o$. Figures 7 and 8, used in conjunction, thus allow one to prescribe a binder burnout cycle in a quantitative manner.

The specification of the threshold value of $(P/P_o)_o$ deserves further comment. In general, the stress at which a body will fail is *a priori* unknown and is an irreversible thermodynamic property that requires destruction of the MLC body. The stress at which the body fails is also not related directly to $(P/P_o)_o$, but rather to the gradient in pressure within the body. We have shown in another work[17] that the six components of stress scale with $(P/P_o)_o$, and thus this ratio, can be used as an indicator of stress within the body.

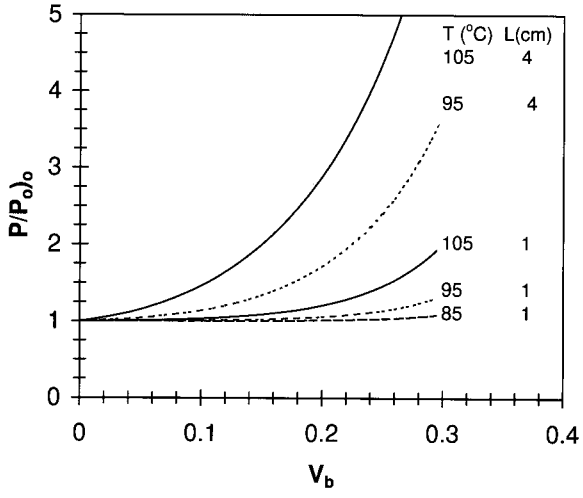

Fig. 7. Simulated pressure ratio at the center of the body versus volume fraction of binder as a function of hold temperature and body length.

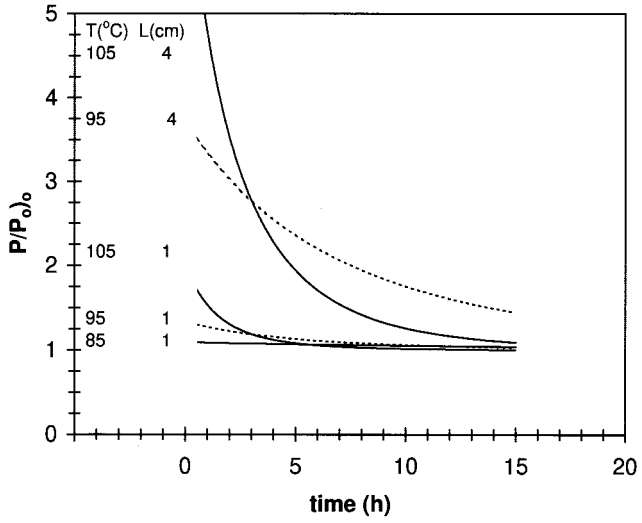

Fig. 8. Simulated pressure ratio at the center of the body versus hold time as a function of hold temperature and body length.

In principle, one can establish the failure stress of a green body by fabricating specimens for strength testing. With this approach, however, the applied load does not arise in the manner of a pressure gradient (an internal body force). We have adopted a different strategy to obtain a value for $(P/P_o)_o$ where we take a set of green samples and decompose the binder at a constant heating rate and monitor the temperature at which the samples fail. This temperature is then used in conjunction with the transport model to establish the threshold value of $(P/P_o)_o$. The binder burnout cycle can then be specified using the methodology inherent in Figs. 7 and 8; this approach[15,28] has been used to develop binder burnout cycles of 25–50 h for MLC samples of 3.8 cm by 3.8 cm by 1.3 cm.

With the concept of a threshold pressure, the strategy embodied by Figs. 7 and 8 suggests that a sequence of ramps and holds can be used to develop cycles for binder removal. We can now extend this methodology to determine the minimum cycle time, t^*, to remove the binder. For the reaction of binder of volume fraction, V_b, into degradation products, p,

$$V_b \rightarrow p \tag{11}$$

the rate, $r(V_b,t)$, can be expressed as

$$\frac{dV_b}{dt} = -r(V_b, t) \tag{12}$$

We can formally integrate Eq. (12) from $t = 0$, $V_b = V_{b,o}$ at $T = T_o$ to $t = t^*$, $V_b = 0$ at $T = T^*$, and solve for time, t^*, as

$$t^* = \int_0^{V_{b,o}} \frac{dV_b}{r(V_b, t)} \tag{13}$$

The specification of the heating profile that determines $r(V_b,t)$ so that t^* is a minimum is a problem of variational calculus.[29] The function $r(V_b,t)$ corresponding to the minimum time in Eq. (13) is the trivial solution of operating at the highest possible temperature where the decomposition rate is high. However, when a threshold pressure ratio, P_t, exists that cannot be exceeded during the binder burnout cycle, the integral in Eq. (13) must be minimized while simultaneously satisfying the constraint

$$\left(\frac{P}{P_o}\right)_o = P_t \tag{14}$$

evaluated where $(P/P_o)_o = P_t$ at $t = 0$ and for all times. The integral in Eq. (14) thus corresponds to varying the heating rate in

such a fashion that the pressure in the center of the body always corresponds to the threshold value so failure does not occur.

The minimum times t^* were determined from solution of Eqs. (13) and (14) as a function of characteristic body dimension and different threshold pressures. Figure 9 indicates that for a given threshold pressure, the heating cycle corresponding to the minimum time arises from a continuous increase in the temperature with time. This functional dependence occurs because as binder is decomposed, the pore space becomes more open, and the sample can be subjected to a higher temperature while still keeping the pressure at the threshold value. Figure 9 further illustrates that for higher values of the threshold pressure, the total cycle times are short; this arises because the sample can be exposed to high temperatures where the degradation kinetics are faster.

Other values of t^* are contained in Table II for bodies of different values of L. For samples of small L, the minimum cycle times are short. As L increases, the minimum time increases as well for the same threshold pressure. For a body of $L = 1$ cm and a threshold pressure ratio of $P_t = 1.1$, the minimum time is 22 h. When the same body is held at a constant temperature of 85.5°C where $P_t = 1.1$ at $t = 0$, the cycle time is 330 h; this comparison illustrates the dramatic effect that varying the temperature in a continuous fashion can have on the duration of the binder burnout cycle.

The initial heating rates, β_o (the tangent to the curves in Fig. 9 as $t \rightarrow 0$), for each sample size and threshold pressure are also listed in Table II. The initial heating rates are seen to increase with increasing threshold pressure and decreasing length. For small values of the threshold pressure, the initial heating rates are very small; this heating rate, however, is not maintained constant throughout the cycle and, as binder is removed, the heating rates can be increased as the pore space becomes more open and the flow of gas out of the body is facilitated. At high values of the threshold pressure, short-cycle times are obtained and these cycles are so short that gradients in temperature and binder content may arise within the body. This more complicated case can then be evaluated by using the full set of equations for the coupled heat and mass transfer[13,15] in conjunction with Eqs. (13) and (14).

The initial heating rates in Table II for $P_t = 1.1$ are of the same order of magnitude as those determined in Refs. 7–9 for bodies of equivalent dimensions. The underlying transport model for those cases, however, is derived for porous bodies highly loaded with binder for which the rate-limiting transport step is diffusion of the decomposition products through the remaining binder fraction. In Refs. 7–9, a critical heating rate was defined as the constant heating rate corresponding to maintaining the maximum vapor pressure below ambient pressure. Nonlinear temperature profiles were not considered, but presumably in the early part of the heating cycle, where the vapor pressure is low, faster heating rates

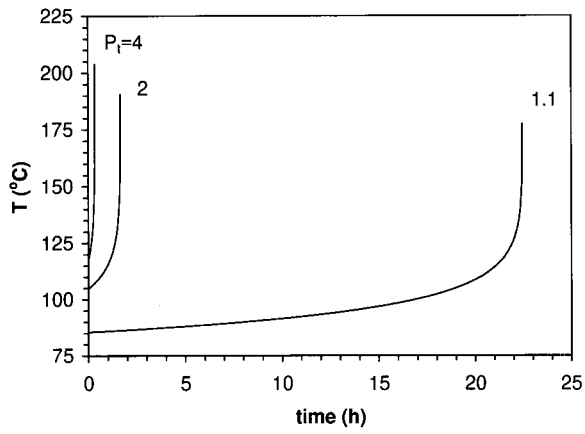

Fig. 9. Temperature profiles with time calculated by using the method of variational calculus as a function of threshold pressure for a body of $L = 1$ cm.

Table II. Minimum Cycle Time, Initial Furnace Temperature, and Initial Heating Rate for Different Threshold Pressures as a Function of Sample Dimension

P_t	T_s(°C)	t^* (h)	β_o (°C/s)
		$L = 2$ cm	
4	106.7	1.3	2×10^{-3}
2	94.5	6.4	5×10^{-4}
1.1	76.1	87.5	3×10^{-5}
		$L = 1$ cm	
4	117.8	0.34	1×10^{-2}
2	104.9	1.7	2×10^{-3}
1.1	85.5	22	1×10^{-4}
		$L = 0.5$ cm	
4	129.5	0.1	4×10^{-2}
2	115.9	0.5	8×10^{-3}
1.1	95.4	6.0	5×10^{-4}

can be used, compared with later in the cycles when the temperature, and thus vapor pressure, are higher. In fact, this strategy was used in that the critical heating rate was not used for the entire heating cycle but only for the portion of the cycle identified to be critical for maintaining the integrity of the samples. The heating profile corresponding to the minimum time can be established by using the method of variational calculus described here, but modified to use the governing equations for their case.

The approach to determine the minimum cycle time with Eqs. (13) and (14) was applied in this work for the specific case of a constant-threshold pressure. The method, however, is general, and when the threshold pressure is not a constant but rather varies with time, $P_t(t)$, this dependency can be incorporated into the constraint (Eq. (14)) as well. Such a dependence may be valid because the strength of a green body is a strong function of the binder content.

The strategy proposed here for developing binder burnout cycles can be compared with the process control strategy of monitoring weight loss within the furnace and then varying the temperature so that the rate of weight loss is kept below some prescribed value.[30,31] Both methods are based on a heuristic; in our case on the threshold pressure and for the other on the rate of weight loss. The latter method can also be used on samples of different length, as long the feedback rate of weight loss is from samples of the same dimension as the actual components being subjected to binder removal. The method proposed here does not require modifications to furnaces but instead is model based and provides some insight into the coupled effects of kinetics, body size, and heating cycle. A final comment pertains to the practical limitation of most temperature controllers, which do not allow one to prescribe a continuous function for the heating cycle. To circumvent this, a sequence of ramps and soaks can be used to approximate the heating profile as being piecewise linear.

IV. Conclusions

The dependence of binder weight loss on the heating rate used in thermogravimetric analysis experiments has been illustrated. It was demonstrated that, even in the absence of a precise degradation mechanism, values for the pre-exponential factor and activation energy can be determined that provide a reasonable representation of the rate of binder decomposition. These values, however, may not be accurate for predicting the rate of binder weight loss when used at temperatures far removed from the corresponding experimental data.

The values of the pre-exponential factor and activation energy were used in a coupled transport and kinetic model to predict the evolution of pressure in the ceramic green body as a function of time, temperature, and dimension of the body. With this strategy, it was demonstrated how one can specify a binder burnout cycle in a quantitative manner. Finally, a method based on calculus of

variations was developed to determine the minimum cycle time for binder removal. This approach can be used for green ceramic bodies where the degradation of binder occurs as a rate process and where failure is attributed to the buildup of pressure within the pore space of the body.

References

[1]J. A. Lewis, "Binder Removal from Ceramics," *Annu. Rev. Mater. Sci.*, **27**, 147–73 (1997).

[2]H. H. G. Jellinek, "Degradation and Depolymerization Kinetics"; pp. 1–37 in *Aspects of Degradation and Stabilization of Polymers*. Edited by H. H. G. Jellinek. Elsevier, New York, 1978.

[3]C. David, *Comprehensive Chemical Kinetics: Degradation of Polymers*, Vol. 14; Ch. 1. Edited by C. H. Gamford and C. F. H. Tipper. Elsevier, New York, 1975.

[4]D. W. Spronson and G. L. Messing, "Organic Binder Removal Processes in Closed Pore Powder-Binder Systems: pp. 528–37 in *Ceramic Powder Science II, Part A*. Edited by G. L. Messing, E. Fuller, and H. Hausner. American Ceramic Society, Columbus, OH, 1988.

[5]M. R. Barone and J. C. Ulicny, "Liquid-Phase Transport during Removal of Organic Binders in Injection-Molded Ceramics," *J. Am. Ceram. Soc.*, **73**, 3323–33 (1990).

[6]P. Calvert and M. Cima, "Theoretical Models for Binder Burnout," *J. Am. Ceram. Soc.*, **73**, 575–79 (1990).

[7]J. R. G. Evans, M. J. Edirisinghe, J. K. Wright, and J. Crank, "On the Removal of Organic Vehicle from Moulded Ceramic Bodies," *Proc. R. Soc. London, A*, **432**, 321 (1991).

[8]J. H. Song, M. J. Edirisinghe, J. R. G. Evans, and E. H. Twizell, "Modeling the Effect of Gas Transport on the Formation of Defects during Thermolysis of Powder Moldings," *J. Mater. Res.*, **11**, 830–40 (1996).

[9]S. A. Matar, M. J. Edirisinghe, J. R. G. Evans, and E. H. Twizell, "Diffusion of Degradation Products in Ceramic Moldings during Thermal Pyrolysis: Effect of Geometry," *J. Am. Ceram. Soc.*, **79**, 749–55 (1996).

[10]R. M. German, "Theory of Thermal Debinding," *Int. J. Powder Metall.*, **23** [4] 237–45 (1987).

[11]G. Y. Stangle and I. A. Aksay, "Simultaneous Momentum, Heat and Mass Transfer with Chemical Reaction in a Disordered Porous Medium: Application to Binder Removal from a Ceramic Green Body," *Chem. Eng. Sci.*, **45**, 1719–31 (1990).

[12]D.-S. Tsai, "Pressure Buildup and Internal Stresses during Binder Burnout: Numerical Analysis," *AIChE J.*, **37**, 547–54 (1991).

[13]A. C. West and S. J. Lombardo, "The Role of Thermal and Transport Properties on the Binder Burnout of Injection Molded Ceramic Components," *Chem. Eng. J.*, **71**, 243–52 (1998).

[14]T. S. Shivashankar and R. M. German, "Effective Length Scale for Predicting Solvent-Debinding Times of Components Produced by Powder Injection Molding," *J. Am. Ceram. Soc.*, **82**, 1146–52 (1999).

[15]L. C.-K. Liau, B. Peters, D. S. Kruger, A. Gordon, D. S. Viswanath, and S. J. Lombardo, "The Role of Length Scale on Pressure Increase and Yield of PVB–$BaTiO_3$–Pt Multi-Layer Ceramic Capacitors during Binder Burnout," *J. Am. Ceram. Soc.*, **83,** 2645–53 (2000).

[16]S. J. Lombardo and Z. C. Feng, "A Model for Pressure Distribution during Binder Burnout in Three-Dimensional Porous Ceramic Bodies with Anisotropic Permeability," submitted to *J. Appl. Mech*..

[17]Z. C. Feng, B. He, and S. J. Lombardo, "Pressure Distribution during Binder Burnout in Three-Dimensional Porous Ceramic Bodies with Anisotropic Permeability," to appear in *J. Appl. Mech*.

[18]S. Madorsky and S. Strauss, "Thermal Degradation of Polyethylene Oxide and Polypropylene Oxide," *J. Polym. Sci.*, **36**, 183–94 (1959).

[19]K. E. Hrdina, J. W. Halloran, A. Oliveira, and M. Kaviany, "Chemistry of Removal of Ethylene Vinyl Acetate Binders," *J. Mater. Sci.*, **33**, 2795–803 (1998).

[20]L. C. K. Liau, T. C. K. Yang, and D. S. Viswanath, "Mechanism of Degradation of Poly (Vinyl Butyral) Using Thermogravimetry/Fourier Transform Infrared Spectrometry," *Polym. Eng. Sci.*, **36**, 2589–600 (1996).

[21]P. A. Redhead, "Thermal Desorption of Gases," *Vacuum*, **12**, 203–11 (1962).

[22]T. V. Lee and S. R. Beck, "A New Integral Approximation Formula for Kinetic Analysis of Nonisothermal TGA Data," *AIChE J.*, **30**, 517–19 (1984).

[23]T. C. K. Yang, W. H. Chang, and D. S. Viswanath, "Thermal Degradation of Poly(Vinyl Butyral) in Alumina, Mullite and Silica Composites," *J. Therm. Anal.*, **47**, 697–713 (1996).

[24]R. J. Cvetanovic and Y. Amenomiya, "A Temperature Programmed Desorption Technique for Investigation of Practical Catalysts," *Catal. Rev.***, 6**, 21–48 (1972).

[25]S. J. Lombardo and A. T. Bell, "A Review of Theoretical Models of Adsorption, Diffusion, Desorption, and Reaction of Gases on Metal Surfaces," *Surf. Sci. Rep.*, **13**, 1–72 (1991).

[26]G. P. Brown, A. DiNardo, G. K. Cheng, and T. K. Sherwood, "The Flow of Gases in Pipes at Low Pressures," *J. Appl Phys.*, **17**, 802–13 (1946).

[27]N. Wakao, S. Otani, and J. M. Smith, "Significance of Pressure Gradients in Porous Materials: Part I. Diffusion and Flow in Fine Capillaries," *AIChE J.*, **11**, 435–39 (1965).

[28]B. Peters and S. J. Lombardo, "Optimization of Multi-Layer Ceramic Capacitor Geometry for Maximum Yield during Binder Burnout," *J. Mater. Sci., Materials in Electronics*, **12**, 403–409 (2001).

[29]M. M. Denn, *Optimization by Variational Methods*. McGraw-Hill, New York, 1969.

[30]A. Johnsson, E. Carlström, L. Hermansson, and R. Carlsson, "Rate-Controlled Extraction Unit for Removal of Organic Binders from Injection-Molded Ceramics," *Mater. Sci. Monogr.*, **16**, 767–72 (1983).

[31]H. Verweij and W. H. M. Bruggink, "Reaction-Controlled Binder Burnout of Ceramic Multilayer Capacitors," *J. Am. Ceram. Soc.*, **73**, 226–31 (1990). □